JACS
JOURNAL OF THE AMERICAN CHEMICAL SOCIETY

ARTICLE

pubs.acs.org/JACS

Oxidative-Stability Enhancement and Charge Transport Mechanism in Glyme–Lithium Salt Equimolar Complexes

Kazuki Yoshida,[†] Megumi Nakamura,[†] Yuichi Kazue,[†] Naoki Tachikawa,[†] Seiji Tsuzuki,[‡] Shiro Seki,[§] Kaoru Dokko,[†] and Masayoshi Watanabe*[,†]

[†]Department of Chemistry and Biotechnology, Yokohama National University, 79-5 Tokiwadai, Hodogaya-ku, Yokohama 240-8501, Japan

[‡]National Institute of Advanced Industrial Science and Technology (AIST), Tsukuba Central 2, Tsukuba, Ibaraki 305-8568, Japan

[§]Materials Science Research Laboratory, Central Research Institute of Electric Power Industry (CRIEPI), 2-11-1 Iwado-kita, Komae, Tokyo 201-8511, Japan

Supporting Information

ABSTRACT: The oxidative stability of glyme molecules is enhanced by the complex formation with alkali metal cations. Clear liquid can be obtained by simply mixing glyme (triglyme or tetraglyme) with lithium bis(trifluoromethylsulfonyl)-amide (Li[TFSA]) in a molar ratio of 1:1. The equimolar complex [Li(triglyme or tetraglyme)$_1$][TFSA] maintains a stable liquid state over a wide temperature range and can be regarded as a room-temperature ionic liquid consisting of a [Li(glyme)$_1$]$^+$ complex cation and a [TFSA]$^-$ anion, exhibiting high self-dissociativity (ionicity) at room temperature. The electrochemical oxidation of [Li(glyme)$_1$][TFSA] takes place at the electrode potential of ~5 V vs Li/Li$^+$, while the oxidation of solutions containing excess glyme molecules ([Li(glyme)$_x$]-[TFSA], $x > 1$) occurs at around 4 V vs Li/Li$^+$. This enhancement of oxidative stability is due to the donation of lone pairs of ether oxygen atoms to the Li$^+$ cation, resulting in the highest occupied molecular orbital (HOMO) energy level lowering of a glyme molecule, which is confirmed by ab initio molecular orbital calculations. The solvation state of a Li$^+$ cation and ion conduction mechanism in the [Li(glyme)$_x$][TFSA] solutions is elucidated by means of nuclear magnetic resonance (NMR) and electrochemical methods. The experimental results strongly suggest that Li$^+$ cation conduction in the equimolar complex takes place by the migration of [Li(glyme)$_1$]$^+$ cations, whereas the ligand exchange mechanism is overlapped when interfacial electrochemical reactions of [Li(glyme)$_1$]$^+$ cations occur. The ligand exchange conduction mode is typically seen in a lithium battery with a configuration of [Li anode|[Li(glyme)$_1$][TFSA]|LiCoO$_2$ cathode] when the discharge reaction of a LiCoO$_2$ cathode, that is, desolvation of [Li(glyme)$_1$]$^+$ and insertion of the resultant Li$^+$ into the cathode, occurs at the electrode–electrolyte interface. The battery can be operated for more than 200 charge–discharge cycles in the cell voltage range of 3.0–4.2 V, regardless of the use of ether-based electrolyte, because the ligand exchange rate is much faster than the electrode reaction rate.

1. INTRODUCTION

Ethers have high donor numbers and relatively strong Lewis basicity due to the lone pair of oxygen atoms in their structure, which results in a high ability to dissociate alkali metal salts through strong solvation to cations. Even polyethers, typically poly(ethylene oxide), can dissolve alkali metal salts such as $LiClO_4$, etc., and the resultant polymer electrolytes show appreciable ionic conductivity under ambient conditions.[1−4] To this end, ethers are attractive as solvents of aprotic electrolytes to be used in electrochemical devices.[5−8] Ionic conductivity of electrolytes is especially important for electrochemical energy storage devices such as lithium batteries, because the power densities of the devices are significantly influenced by conductivity. In addition to mass transport in the electrolytes, charge-transfer processes take place at the electrode/electrolyte interface. As a result, the physicochemical properties of electrolytes have a significant effect on the performance of the devices. It is therefore necessary for the promotion of energy efficiency to develop new functional electrolytes that have desirable properties for practical applications.

To date, lithium secondary batteries, which use aprotic electrolytes, are one of the most important energy storage devices. They have high energy density for use in portable electronic devices and electric vehicles.[9−11] However, despite their high solvation ability for salt dissociation, ethers have not been utilized in practical lithium secondary batteries. This is because the extraction of electrons from the lone pair of oxygen atoms causes the oxidation of ethers to take place at an electrode potential higher than 4 V vs Li/Li$^+$, and they are not compatible with 4 V class cathode materials such as $LiCoO_2$ and $LiMn_2O_4$.[12,13] Instead of ethers, carbonate solvents (cyclic and linear carbonates) with dissolved lithium salts such as $LiPF_6$ are used in practical lithium batteries.[14]

Room-temperature ionic liquids (RTILs), consisting of entirely cations and anions, are also important new electrolyte candidates. They may be applicable to electric double-layer

Received: April 30, 2011
Published: July 20, 2011

capacitors,[15,16] fuel cells,[17−19] dye-sensitized solar cells,[20−22] and lithium-ion batteries (LIBs)[23−35] to achieve high thermal stability in the electrochemical devices. One of the major strategies for using RTILs as electrolytes for LIBs is to use them instead of organic solvents as a solvent for Li salts. Although these electrolytes are liquid at room temperature and have a high thermal stability, there are certain drawbacks, including low Li^+ cation concentration, low Li^+ cation transference number, and concentration polarization during charge−discharge.[36] With the aim of establishing an alternate strategy for obtaining Li^+ cation-conducting RTILs, we have reported the preparation of lithium ionic liquids consisting of lithium salts of borates having electron-withdrawing groups (to reduce the anionic basicity) and lithium-coordinating ether ligands (to dissociate the lithium cations from the anionic centers). However, possibly due to the strong Lewis acidity of Li^+, the ionicity (dissociativity) of the lithium ionic liquids at room temperature is as low as 0.1−0.3; due to high viscosity, ionic conductivity is 10^{-5}−10^{-4} S cm^{-1}.[37,38]

Recently, we found that the equimolar complexes of glymes (oligoethers) and Li salts, which maintain a liquid state at room temperature, can be used as electrolytes for 4 V class lithium batteries.[39] It is well-known that glymes such as triglyme (G3) and tetraglyme (G4) form one-to-one complexes with certain Li salts, and their crystallographic structures and thermal properties have been investigated extensively.[40−43] Furthermore, crystalline oligoether(glyme)−Li salt complexes were also reported as possible candidates for new crystalline solid electrolytes.[44−49] Our group has focused on the transport properties and electrochemical properties of fused complexes that consist of equimolar mixtures of a glyme molecule (G3 or G4) and a Li salt.[50] The glyme−Li salt equimolar complexes demonstrate low volatility, high thermal stability, high ionic conductivity, and a wide potential window, and they behave like conventional RTILs.[50]

There are distinct differences between the glyme−Li salt equimolar complexes and conventional RTILs with added lithium salts. In the complexes, the Li^+ cation is involved in the formation of a $[Li(glyme)_1]^+$ cation,[50] and the ionic conductivity is as high as 10^{-3} S cm^{-1} due to the high dissociativity (0.6−0.7) and high concentration (∼3 mol dm^{-3}) of the complex at room temperature.[50] Furthermore, the glyme−Li salt equimolar complexes exhibit higher oxidative stability than do glyme/Li salt solutions containing excess glyme molecules.[50] Because of the donation of lone pairs of ether oxygen to the Li^+ cation, it appears that the extraction of electrons from the lone pairs of $[Li(glyme)_1]^+$ complex cation becomes more difficult than that of free glyme. Therefore, the glyme−Li salt equimolar complexes are presumed to be resistive against oxidation, and they are thought to be promising electrolytes for 4 V class lithium batteries. In this study, the oxidative stability of the equimolar glyme−Li salt fused complexes was investigated by means of electrochemical techniques and ab initio molecular orbital calculations. Furthermore, $[Li(glyme)_1][TFSA]$ complexes were adopted as electrolyte of the [Li anode|$[Li(glyme)_1][TFSA]$|$LiCoO_2$ cathode] cell. Interestingly, the cell could be charged and discharged for more than 200 cycles with high Coulombic efficiencies and high-capacity retentions, although the free glyme molecules were released (desolvated) at the cathode interface when discharging. The ligand exchange rate constants of $[Li(glyme)_1]^+$ complex cation and free glyme were elucidated by means of ^{1}H NMR. The high cyclability was interpreted in terms of the rate of the ligand exchange reaction being sufficiently higher than that of the charge-transfer reaction at the $[Li(glyme)_1][TFSA]|LiCoO_2$ cathode interface. Finally, we propose the Grotthuss-like mechanism of the ligand exchange reaction (Li^+ cation conduction) in the glyme−Li salt equimolar complexes, which is induced by the electrochemical reactions at the electrode interfaces.

2. EXPERIMENTAL SECTION

Purified G3 or G4 (Kishida Chemical) and Li[TFSA] (Sumitomo 3M) were mixed in a glovebox filled with argon gas (VAC, $[H_2O]$ < 1 ppm). The mixtures were stirred for 24 h at room temperature, and homogeneous liquids were obtained. The liquids were stored and handled in the glovebox. The liquids are abbreviated as $[Li(glyme)_x][TFSA]$, where the molar ratio of glyme:Li[TFSA] = x:1. The residual water in the glyme−lithium salt mixtures was measured using a Karl Fischer moisture meter (Mitsubishi CA-07), and it was below 30 ppm for each liquid.

^{1}H NMR measurements for glyme−lithium salt mixtures were performed on a JEOL JNM-AL 400 spectrometer using an NMR double-tube and $CDCl_3$ as an external standard. The NMR spectra were collected at 30 °C.

The electrochemical stabilities of $[Li(glyme)_x][TFSA]$ (x = 1, 4, 8, and 20) were evaluated by linear sweep voltammetry (LSV) with two electrode cells. The counter and reference electrode is lithium, and the working electrode is platinum.

Using the $[Li(glyme)_x][TFSA]$ electrolyte (x = 1 and 4), [Li metal anode|$[Li(glyme)_x][TFSA]|LiCoO_2$ cathode] cells were constructed, and the charge−discharge characteristics were tested. The cathode layer was composed of $LiCoO_2$ (85 wt %, AGC Seimi Chemical) as a cathode-active material, acetylene black (9 wt %, Denki Kagaku Kogyo) as an electrically conductive additive, and poly(vinylidene fluoride) (6 wt %, Kureha Chemical) as a binder polymer. These materials were mixed together and thoroughly agitated in *N*-methylpyrrolidone with a homogenizer. The obtained slurry was applied with an automatic applicator onto an aluminum current collector, and the resulting cathode sheet was dried at 100 °C. Next, the cathode sheet was compressed using a roll press machine to improve electrical conductivity (electrode thickness 15 μm, electrode loading 3 mg cm^{-2}). The cathode sheet, a separator, $[Li(glyme)_x][TFSA]$ electrolyte, and a Li metal anode were encapsulated into a 2032-type coin cell in the glovebox. To ensure complete swelling of the electrolyte into the pressed cathode sheet, the fabricated battery was aged at 60 °C for more than 18 h. Charge−discharge tests of the cells were performed at 3.0−4.2 V, with a current density of 50 μA cm^{-2} (1/8 C-rate) at 30 °C.

The electrochemical impedance measurements for the cells were carried out with a peak-to-peak amplitude of 10 mV and frequency ranging from 500 kHz to 20 mHz. All electrochemical measurements were conducted using an electrochemical measurement system (Princeton Applied Research, VMP2) at 30 °C.

The Gaussian 03 program[51] was used for the ab initio molecular orbital calculations. The basis sets implemented in the Gaussian program were used. The geometries of the glymes (G3 and G4) and their complexes were fully optimized at the HF/6-311G** level. The HOMO energy levels were calculated at the HF/6-311G** level.

3. RESULTS AND DISCUSSION

Oxidative-Stability Enhancement in Glyme−Lithium Salt Equimolar Complexes. Figure 1 shows LSVs of $[Li(glyme)_x][TFSA]$ measured at 30 °C. The anodic current for the electrolytes is observed at an electrode potential higher than 4 V vs Li/Li^+. As the molar ratio (x) of the glymes decreases in the electrolytes, the anodic limit shifts to a more positive potential. It is known that the anodic limit of ether electrolytes is about 4 V vs Li/Li^+. The oxidative decomposition of ether electrolytes arises

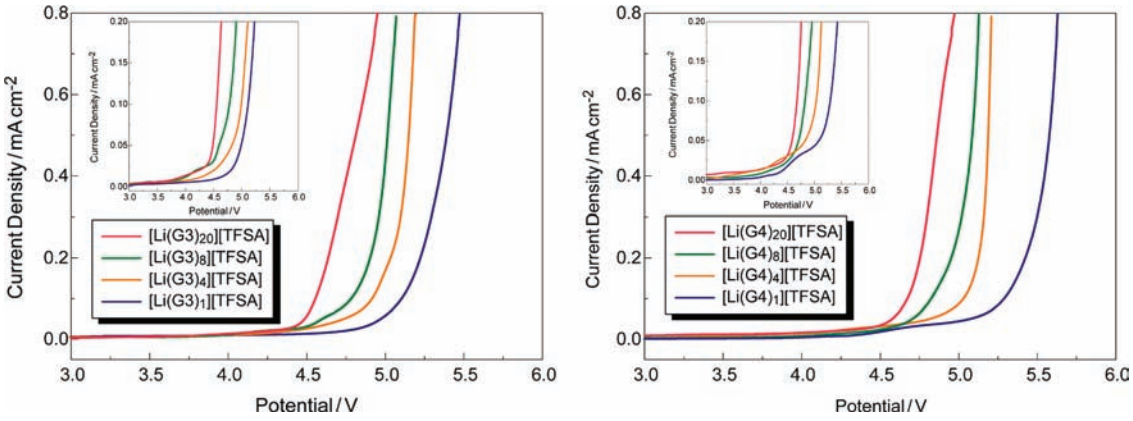

Figure 1. Linear sweep voltammograms of $[Li(glyme)_x][TFSA]$ (x = 1, 4, 8, and 20) at a scan rate of 1 mV s^{-1} at 30 °C. Each inset depicts an enlarged view of current density.

from oxidation of the oxygen atoms. Indeed, irreversible oxidative currents for both $[Li(G3)_{20}][TFSA]$ and $[Li(G4)_{20}][TFSA]$ started to flow at around 4 V vs Li/Li^+. The oxidative limits of equimolar complexes ($[Li(glyme)_1][TFSA]$) are close to 5 V vs Li/Li^+ and are apparently higher than the other electrolytes. It is assumed that the free glymes, which are not involved in the complexation with Li^+ in $[Li(glyme)_x][TFSA]$ ($x > 1$), are oxidized at higher than 4 V vs Li/Li^+. The glyme donates lone pairs to the Li^+ cation, resulting in the enhancement of oxidative stability of the ether structure. As the molar ratio (x) of the glymes increases in the solution, the concentration of the free glyme is increased and the oxidation current increases, which leads to a lower anodic limit. In the case of equimolar complex ($[Li(G3 \text{ or } G4)_1][TFSA]$), all glyme molecules form complex cations with Li^+, and the oxidation limit becomes much higher than the electrolytes containing excess glymes.

The weakly Lewis-acidic complex cation $[Li(glyme)_1]^+$ can be obtained through the donation of lone pairs of a glyme molecule (Lewis base) to a Li^+ cation (Lewis acid). Because of the formation of the complex, the Lewis acidity of Li^+ is greatly weakened, which is a concept analogous to the formation of a weakly Lewis-basic anion such as BF_4^- and PF_6^- by the reaction between a Lewis acid (BF_3 or PF_5) and a Lewis base (F^-). The combination of a weakly Lewis-acidic complex cation $[Li(glyme)_1]^+$ and a weakly Lewis-basic $[TFSA]^-$ anion leads to ionic dissociation in the fused complex even in the absence of excess glyme molecules, similarly to conventional RTILs.[52−55] In addition, we have found that the vapor pressure of $[Li(glyme)_1][TFSA]$ is negligible at temperatures lower than 100 °C.[50] Furthermore, the self-diffusion coefficients of the glyme (D_{sol}) and Li^+ cation (D_{Li}) in glyme−Li salt complexes, which were measured by pulsed-field gradient spin−echo NMR (PGSE-NMR), are the same within experimental error.[50] The identical values of D_{sol} and D_{Li} in the glyme−Li salt complexes strongly indicate that each Li^+ cation is coordinated by a glyme molecule, and that they diffuse together as a complex cation $[Li(glyme)_1]^+$ in the liquid. From these features, the equimolar complexes can be regarded as ionic liquids consisting of $[Li(glyme)_1]^+$ complex cation and a $[TFSA]^-$ anion.

Ab initio molecular orbital calculations were performed to enable a detailed discussion of the oxidative stability of $[Li(glyme)_1][TFSA]$. The optimized structures for the $[Li(G3)_1][TFSA]$ and $[Li(G4)_1][TFSA]$ complexes are shown in Figure 2. The initial geometries of the complexes used for geometry optimizations were prepared on the basis of the crystal structures.[41,42]

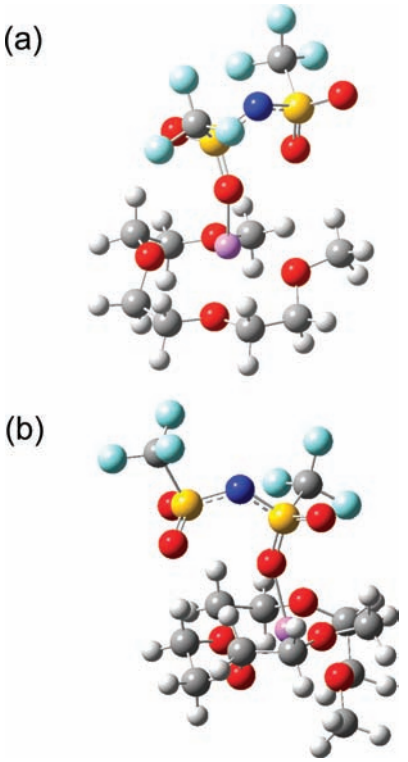

Figure 2. Optimized structures of $[Li(G3)_1][TFSA]$ (a) and $[Li(G4)_1][TFSA]$ (b). Purple, Li; red, O; silver, C; blue, N; yellow, S; light blue, F; white, H.

The glyme donates lone pairs of oxygen atoms to the Li^+ cation, and the glyme molecule wraps around the Li^+ cation to form a complex cation $[Li(glyme)_1]^+$. The optimized structure of the $[Li(G3)_1][TFSA]$ shown in Figure 2a is close to the structure of $[Li(G3)_1][N(SO_2C_2F_5)_2]$ in the crystalline state reported by Henderson et al.[42] The Li−O distances in the $[Li(G3)_1][TFSA]$ calculated in this work (2.035−2.210 Å) are close to those in the crystal of $[Li(G3)_1][N(SO_2C_2F_5)_2]$ (1.978−2.156 Å). Regarding the 1:1 complex of G4 and a Li salt, Henderson et al. reported the formation of double-helix dimer, $[Li_2(G4)_2]^{2+}$, for the crystal structure of G4:$LiAsF_6$ = 1:1.[41] The HF/6-311G** level optimized geometry of $[Li_2(G4)_2]^{2+}$ was also carried out here as a possible structure and is shown in the Supporting Information

Table 1. HOMO Energy Levels Calculated for G3, $[Li(G3)_1]^+$, $[Li(G3)_1][TFSA]$, G4, $[Li(G4)_1]^+$, and $[Li(G4)_1][TFSA]$

HOMO energy level	atomic unit	eV
G3 (*all trans*)	−0.42093	−11.45
$[Li(G3)_1]^+$	−0.57001	−15.51
$[Li(G3)_1][TFSA]$	−0.44483	−12.10
G4 (*all trans*)	−0.42116	−11.46
$[Li(G4)_1]^+$	−0.54742	−14.90
$[Li(G4)_1][TFSA]$	−0.43357	−11.80

(Figure S1). The complex structure may change depending on anion species, molar ratio of Li:G4 in the mixture,[41] and also liquid or solid. In the present study, $[Li(G3 \text{ or } G4)_1][TFSA]$ is liquid at room temperature, and the transport properties of the liquid are strongly influenced by the complex structure. If Li^+ and the glyme form a 2:2 complex in the liquid, the hydrodynamic radius of $[Li_2(glyme)_2]^{2+}$ and the Coulomb interaction with the anion should be much larger than those of $[Li(G4)_1]^+$ and $[Li(G3)_1]^+$, which would lead to a high viscosity, a small diffusivity of Li^+, and a smaller transference number of Li^+ than that of $[TFSA]$ anion. However, as reported elsewhere,[50] the viscosity of $[Li(G4)_1][TFSA]$ is smaller than that of $[Li(G3)_1][TFSA]$, and the diffusion coefficient of Li^+ in $[Li(G4)_1][TFSA]$ is larger than that in $[Li(G3)_1][TFSA]$. In addition, the Li^+ transference numbers of $[Li(G3)_1][TFSA]$ and $[Li(G4)_1][TFSA]$ are evaluated to be 0.61 and 0.51, respectively.[50] On the basis of these results, it is postulated that the $[Li_2(glyme)_2]^{2+}$ does not exist in these liquids.

The glyme−Li salt complex formation is analogous to the complex formation between crown ethers and alkali metal (i.e., Li^+, Na^+, and K^+) salts,[56] while the melting temperatures of the latter complexes are much higher than the former and also higher than ambient temperatures. The HOMO energy levels calculated for isolated glyme molecules, $[Li(glyme)_1]^+$ cations, and $[Li(glyme)_1][TFSA]$ complexes are shown in Table 1. Electrochemical oxidation of glyme molecules at the electrode/electrolyte interface occurs when electrons are extracted from the HOMO of glyme. Therefore, substances having a high HOMO energy level are easily oxidized. The HOMO energy levels of isolated G3 and G4 are almost identical. The complexation with a Li^+ cation considerably lowers the HOMO energy levels of glymes. The glyme is highly polarized by the strong electric field of the Li^+ cation, and it donates lone pairs to the Li^+ cation, resulting in the lowering of the HOMO energy level. The calculations support the idea that the Li^+ cation complex formation is effective in improving the oxidation stability of the glyme molecules. The lowering of the HOMO energy levels of G3 or G4 by complex formation is very large (4.1 and 3.4 eV, respectively). The magnitude of the lowering of the HOMO energy level of the $[Li(G3)_1]^+$ cation is larger than that of the $[Li(G4)_1]^+$ cation, probably due to the difference of the polarization of the oxygen atoms. The Li−O distances in the $[Li(G3)_1]^+$ complex are 1.968−2.009 Å, while those in the $[Li(G4)_1]^+$ complex are 2.114−2.189 Å (refer to the Supporting Information). The Li distances in the complexes suggest that the larger polarization of the oxygen atoms in the $[Li(G3)_1]^+$ complex is the cause of the larger magnitude of the lowering of the HOMO energy level. It is also interesting to note that the HOMO energy levels of the glymes in the $[Li(G3 \text{ or } G4)_1][TFSA]$ complexes are substantially higher than those of the $[Li(G3 \text{ or } G4)_1]^+$ cations. In the optimized structures of the $[Li(G3 \text{ or } G4)_1][TFSA]$ complexes, the Li^+ cations have contact with the oxygen atom of the sulfonyl group of the $[TFSA]$ anion, as shown in Figure 2, which suggests that the negatively charged oxygen atom weakens the electric field around the Li^+ cations. This is likely the cause of the higher HOMO energy levels of the $[Li(glyme)_1][TFSA]$ complexes as compared to those of the $[Li(glyme)_1]^+$ cation complexes.

Comparing the voltammograms of $[Li(glyme)_1][TFSA]$ and $[Li(glyme)_{20}][TFSA]$, the enhancement of the anodic limit, that is, oxidative stability, by elimination of free glymes is 0.5−1.0 V, which lies between the predicted values of 3.4−4.1 V for $[Li(glyme)_1]^+$ and those of 0.34−0.65 V for $[Li(glyme)_1][TFSA]$ by ab initio calculations. We have determined the dissociativity (ionicity) of $[Li(G3)_1][TFSA]$ and $[Li(G4)_1][TFSA]$ to be 0.68 and 0.63 at 30 °C, respectively, by PGSE-NMR.[50] If $[Li(glyme)_1]^+$ cations exist in the molten complexes in an equilibrium between the free state and the anion-associated state, the differences between the experimental enhancement of the anodic limit and the calculated values can be understood qualitatively. Although the calculated HOMO levels are only for a single ion or ion pair in vacuum and the effects of the interaction between molecules and other ions are not taken into account, the enhancement of the oxidative stability of the glyme molecule by complexation with the Li^+ cation is in agreement with the results of the linear sweep voltammograms in Figure 1.

The LSVs of the $[Li(G3)_1][TFSA]$ and $[Li(G4)_1][TFSA]$ (Figure 1) are very similar at first glance, and the oxidation current increases rapidly at an electrode potential higher than 5.0 V vs Li/Li^+. However, upon closer inspection (Figure 1, inset) at around 4.3 V vs Li/Li^+, one can notice the onset of oxidation for $[Li(G4)_1][TFSA]$. On the other hand, $[Li(G3)_1]$ $[TFSA]$ shows a very flat voltammogram up to 4.5 V vs Li/Li^+, and the anodic current of $[Li(G3)_1][TFSA]$ is apparently smaller than that of $[Li(G4)_1][TFSA]$ in the potential range from 4.3 to 4.7 V vs Li/Li^+. The slower onset of oxidation of $[Li(G3)_1][TFSA]$ than that of $[Li(G4)_1][TFSA]$ shows good agreement with that of the HOMO energy levels in Table 1, where $[Li(G3)_1]^+$ has a lower HOMO energy than $[Li(G4)_1]^+$, suggesting that $[Li(G3)_1]$ $[TFSA]$ has better oxidative stability than does $[Li(G4)_1][TFSA]$.

Use of Glyme−Lithium Salt Complexes in Lithium Batteries. As demonstrated by LSVs, the equimolar complexes $[Li(G3 \text{ or } G4)_1]$ $[TFSA]$ show good oxidative stability. $[Li(G3)_1]$-$[TFSA]$ and $[Li(G4)_1][TFSA]$ are stable up to 4.5 and 4.3 V vs Li/Li^+, respectively. Furthermore, it has been reported that the electrochemical deposition and stripping of Li metal can be repeated successfully in $[Li(G3)_1][TFSA]$ and $[Li(G4)_1][TFSA]$.[50] Therefore, the equimolar complexes $[Li(G3 \text{ or } G4)_1][TFSA]$ are promising liquid electrolytes for 4 V class lithium batteries. To assess the feasibility of $[Li(G3 \text{ or } G4)_1][TFSA]$ as electrolytes, a [Li anode|$[Li(G3 \text{ or } G4)_1][TFSA]$|$LiCoO_2$ cathode] cell was fabricated and tested. Figure 3 shows galvanostatic charge−discharge curves of [Li anode|$[Li(G3 \text{ or } G4)_1][TFSA]$|$LiCoO_2$ cathode] cells measured in the cell voltage range from 3.0 to 4.2 V. Each cell showed reversible charge−discharge behavior. During the charge, the Li^+ cation deintercalation from the crystallographic structure of the $LiCoO_2$ cathode takes place at an electrode potential higher than 3.9 V vs Li/Li^+, and Li is deposited at the Li anode. The reverse reactions then occur during discharge. In both electrolytes, the $LiCoO_2$ cathode showed an initial discharge capacity of 130 mA h g^{-1}, which is close to the theoretical capacity of 137 mA h g^{-1} of Li_yCoO_2 ($0.5 < y < 1$). The charge−discharge Coulombic efficiency was

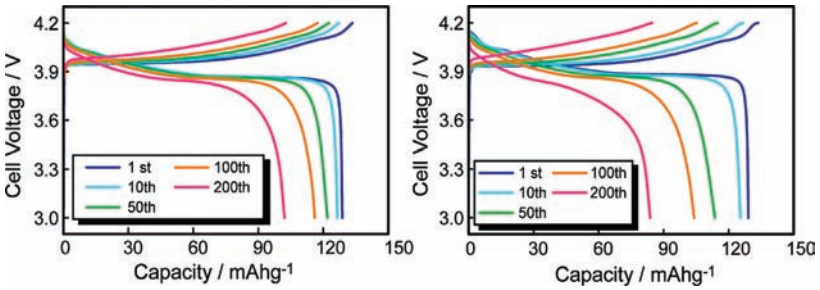

Figure 3. Charge and discharge curves of the [Li metal anode|$[Li(G3)_1][TFSA]$ (left) and $[Li(G4)_1][TFSA]$ (right) electrolyte|$LiCoO_2$ cathode] cells measured with a current density of 50 μA cm^{-2} (1/8 C-rate) at 30 °C.

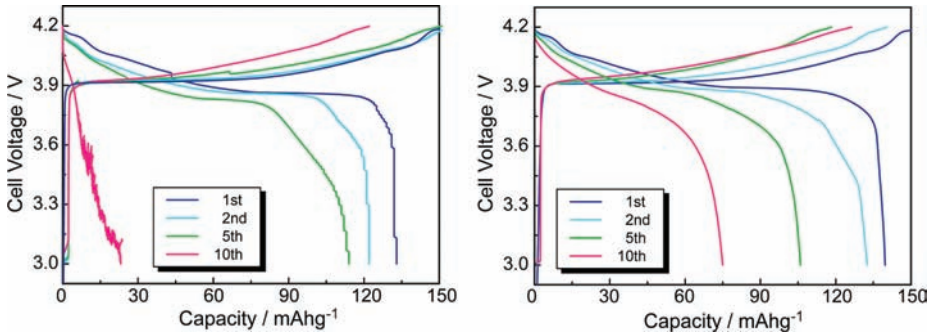

Figure 4. Charge and discharge curves of the [Li metal anode|$[Li(G3)_4][TFSA]$ (left) and $[Li(G4)_4][TFSA]$ (right) electrolyte|$LiCoO_2$ cathode] cells in the first, second, fifth, and 10th cycles measured with a current density of 50 μA cm^{-2} (1/8 C-rate) at 30 °C.

excellent and higher than 95% even at the initial cycle, and higher than 99% at subsequent cycles for both cells. Furthermore, cells with $[Li(G3)_1][TFSA]$ and $[Li(G4)_1][TFSA]$ maintained discharge capacities of 100 and 85 mA h g^{-1}, respectively, even after 200 cycles. These results apparently prove that significant degradations of electrolytes do not take place during the charge−discharge cycles, and they confirm the applicability of the equimolar complexes to 4 V class lithium batteries. In recent decades, it was reported that ether-type electrolytes including polymer electrolytes decompose at electrode potentials higher than 4 V vs Li/Li^+ and cannot be utilized in 4 V class LIBs, taking into account prolonged charge−discharge cycles in practical use.[12,13,57] To the best of our knowledge, this is the first report to show that a 4 V class lithium secondary battery can be operated successfully for more than 200 cycles using ether-based electrolytes. As mentioned before, all of the ether oxygens donate lone pairs to the Li^+ cation in the equimolar complexes, which leads to the extremely improved oxidative stability of the glymes, and the 4 V class cathode can be stably operated in the electrolytes. The cell with $[Li(G3)_1][TFSA]$ shows slightly better cycle stability than the one with $[Li(G4)_1][TFSA]$, which is in good agreement with the results of LSVs in Figure 1 and ab initio molecular orbital calculations in Table 1. $[Li(G4)_1][TFSA]$ shows signs of irreversible oxidation at an electrode potential of 4.3 V vs Li/Li^+, while $[Li(G3)_1][TFSA]$ is stable up to 4.5 V vs Li/Li^+, suggesting that the oxidative stability of $[Li(G3)_1][TFSA]$ is superior to that of $[Li(G4)_1][TFSA]$.

The discharge current density of 50 $\mu A/cm^{-2}$ (1/8 C-rate), shown in Figure 3, is not so high. The rate capability of the cell is also an important property of a battery. We are now investigating the charge−discharge behaviors of the cells at high current densities to correlate with the mass transport process in the electrolytes. Regarding the rate capability, we have achieved at least a 2 C-rate discharge without losing the capacity of $LiCoO_2$ by designing a suitable glyme molecule. For $[Li(G4)_1][TFSA]$, at least a 1 C-rate discharge is possible with a capacity of ca. 130 mA h g^{-1} $LiCoO_2$. Details of the rate capability $[Li|Li(glyme)_1|\ LiCoO_2]$ will be published in a forthcoming paper.

Figure 4 shows the charge−discharge curves of [Li anode|-$[Li(G3\text{ or }G4)_4][TFSA]|LiCoO_2$ cathode] cells (viz., using electrolyte-containing free glyme molecules). The cell with $[Li(glyme)_4][TFSA]$ showed a slightly higher discharge capacity than those with $[Li(glyme)_1][TFSA]$ in the initial cycle. The ionic conductivity of $[Li(glyme)_4][TFSA]$ is higher than that of $[Li(glyme)_1][TFSA]$ (Supporting Information, Table S2). Therefore, the internal resistance of the cell with $[Li(glyme)_4]$-$[TFSA]$ is smaller than that with $[Li(glyme)_1][TFSA]$, leading to that the state of charge of $LiCoO_2$ cathode at 4.2 V in $[Li$-$(glyme)_4][TFSA]$ is higher than that of one in $[Li(glyme)_1][TFSA]$. Consequently, the discharge capacity of the cell with $[Li(glyme)_4]$-$[TFSA]$ was slightly higher than that with $[Li(glyme)_1][TFSA]$. However, the cells with $[Li(glyme)_4][TFSA]$ lose discharge capacities rapidly as the charge−discharge cycle numbers increase. It is speculated that the corrosion of an aluminum current corrector takes place in organic electrolytes containing Li-$[TFSA]$,[58−60] although the Al corrosion mechanism is not clear at present. The rapid loss in the discharge capacity indicates that the irreversible side reactions are enhanced probably due to the increased surface area of Al by the corrosion. The corrosion rate during the initial charge−discharge cycle is probably slower than that of subsequent cycles thanks to the native passivation layer (Al_2O_3) on the Al, resulting in the better Coulombic efficiency of the first cycle than that of subsequent cycles. The fresh and rough surface of Al created by the corrosion may be more active for the

irreversible oxidation of glyme at electrode potentials higher than 4 V and/or Al dissolution, leading to the lower Coulombic efficiency. The corrosion of aluminum will lead to a significant loss of the discharge capacity of the cathode because of the destruction of the current-collecting path from the $LiCoO_2$ particles. On the other hand, [Li anode|[Li(G3 or G4)$_1$][TFSA]|$LiCoO_2$ cathode] cells can be cycled for more than 200 cycles, indicating that the corrosion of aluminum is negligible. The suppression of aluminum corrosion in the equimolar complexes ([Li(glyme)$_1$][TFSA]) is similar to the case of ionic liquid/Li[TFSA] binary electrolytes. It has been well-known that the corrosion of aluminum is suppressed in ionic liquids, regardless of the $[TFSA]^-$ anion in the ionic liquids,[61] and the $LiCoO_2$ cathode can be operated successfully in [TFSA]-based ionic liquids.[26−31,34,35,38] The stability of the passivation layer of the Al surface may change depending on the electrolyte composition, although the aluminum corrosion phenomena due to the $[TFSA]^-$ anion in organic electrolytes and ionic liquid electrolytes are beyond the scope of this work.

Charge Transport Mechanism in Glyme−Lithium Salt Equimolar Complexes under Electrode Reactions. One question arises here from the results of the charge−discharge of cells with electrolytes of [Li(glyme)$_x$][TFSA]. As shown in Figure 4, the cells with electrolytes containing excess glyme molecules, [Li(glyme)$_x$][TFSA] ($x > 1$), cannot be operated stably due to the oxidation of free glymes and the corrosion of the aluminum current collector of the cathode. When the charge−discharge reactions take place in the [Li anode|[Li(G3 or G4)$_1$][TFSA]|$LiCoO_2$ cathode] cell, the solvation/desolvation of the Li^+ cation occurs at the electrode/electrolyte interfaces. This process generates the free-glyme molecules, which are not involved in the complexation, at the cathode interface. Conversely, the Li^+ cation is generated at the Li metal anode during the discharge. It is not realistic to consider that the nonsolvated Li^+ cation and the free-glyme diffuse from the anode and the cathode, respectively, to join and form a complex cation because the self-diffusion coefficient of each species in [Li(glyme)$_x$][TFSA] is in the order of 10^{-7} cm^2 s^{-1},[50] and the distance between the cathode and the anode (separator thickness) is 20 μm, requiring more than 10 s to meet each other in the electrolyte. The free glyme generated at the $LiCoO_2$ cathode should be exposed to oxidative conditions at the cathode during the discharge process of the [Li anode-|[Li(glyme)$_1$][TFSA]|$LiCoO_2$ cathode] cell. If the oxidative reaction of free glyme took place at the cathode, the Coulombic efficiency for the charge−discharge would become very low. This conflicts with the fact that the [Li anode|[Li(glyme)$_1$][TFSA]|$LiCoO_2$ cathode] cell can be operated stably for more than 200 cycles, and good Coulombic efficiency is achieved for the charge−discharge of the cell. The capacity loss observed for the cells with [Li(glyme)$_1$][TFSA] (Figure 3) may be attributed to (i) a parasitic reaction of some portion of the "free" glyme molecules upon release of the lithium cation at the active material interface, (ii) degradation of $LiCoO_2$ cathode, and (iii) increase of electronic resistance of the cathode caused by the break of electron conduction path due to the repetition of a small volume change of $LiCoO_2$ during charge and discharge. Nevertheless, it is reasonable to assume that the considerable oxidation of the free glyme does not occur during battery operation. However, the following question remains: how is the oxidation of the free-glyme at the $LiCoO_2$ cathode prohibited during the discharge process? A possible hypothesis is that the free glyme, which is generated by the discharge reaction at the cathode, receives immediately another Li^+ cation from the neighboring $[Li(glyme)_1]^+$ complex cation and forms again a complex before the oxidation process of the free glyme occurs.

$$glyme^* + [Li(glyme)_1]^+ \rightarrow [Li(glyme^*)_1]^+ + glyme$$

Simultaneously, the Li^+ cation, which is generated by the discharge reaction at the anode, is a strong Lewis acid and takes a glyme away immediately from the neighboring weak Lewis acid $[Li(glyme)_1]^+$. The electrochemical reactions at the anode and the cathode are anticipated to induce the exchange of ligands between complex cations in the electrolytes. Therefore, in addition to the $[Li(glyme)_1]^+$ conduction by the migration (vehicle mechanism), the Li^+ cation conduction due to the exchange of a ligand (glyme molecule), which is induced by the electrochemical reactions in the cell, may take place during discharge of the cell. This conduction mode will propagate over the whole [Li(glyme)$_1$][TFSA] fused complex, as seen in the Grotthuss mechanism[62] for acidic aqueous solutions.

To examine the validity of the aforementioned hypothesis, the states of the $[Li(glyme)_1]^+$ complex cation and the free-glyme molecule in the [Li(glyme)$_x$][TFSA] solution were explored by ^{1}H NMR. Figure 5 shows NMR spectra of the [Li(glyme)$_x$][TFSA] solutions. The assignments of NMR signals are shown in the inset of Figure 5. By dissolving Li[TFSA] into a glyme, the signals became broad and shift to a higher magnetic field. The broadening of the signal is due to the increase in the viscosity of the solution as the concentration of Li[TFSA] increases. Although the signal shift is caused by dissolving Li[TFSA], the free glyme and the glyme bound to the Li^+ cation in the [Li(glyme)$_x$][TFSA] solution cannot be distinguished by ^{1}H NMR. These results indicate that the exchange rate of a ligand of $[Li(glyme)_1]^+$ in the [Li(glyme)$_x$][TFSA] solution is sufficiently fast. In the case of pure glyme, of course, no glyme molecule interacts with the Li^+ cation. On the other hand, in the case of [Li(glyme)$_1$][TFSA] equimolar complexes, each Li^+ cation is coordinated by a glyme molecule, and no free-glyme molecule exists.[50] The lifetime of the free-glyme molecule in the [Li(glyme)$_2$] [TFSA] bulk solution can be estimated from the NMR spectra. When one-half of the glyme molecules join in the coordination with the Li^+ cation in the solution and the exchange of the ligand takes place, the lifetime (τ_b) of the free glyme in [Li(glyme)$_2$][TFSA] can be expressed as follows:[63,64]

$$\tau_b = \frac{2(W - W_0)}{\pi(\delta\nu)^2}$$

where W_0 and W are the full width at half-maximum (fwhm) of the NMR signal of the end methyl proton of pure glyme and [Li(glyme)$_2$] [TFSA], respectively. $\delta\nu$ is the difference in the chemical shift of the end methyl proton of [Li(glyme)$_1$][TFSA] and pure glyme. The estimated τ_b values in [Li(G3)$_2$][TFSA] and [Li(G4)$_2$][TFSA] are 1.9×10^{-4} and 3.6×10^{-4} s, respectively.

To compare the lifetime of free glyme in the bulk solution and the time scale of the charge-transfer process at the electrochemical interface, electrochemical impedance measurements for the Li anode [Li(glyme)$_1$][TFSA] $LiCoO_2$ cathode cell were performed. Figure 6 shows Nyquist plots of the [Li anode|[Li-(glyme)$_1$][TFSA]|$LiCoO_2$ cathode] cells measured at the cell voltage of 4 V. Two depressed semicircles can be seen in each Nyquist plot. From the peak frequency (f_{max}) of each semicircle, the time constant [$\tau_i = 1/(2\pi f_{max})$] for the charge transfer at the

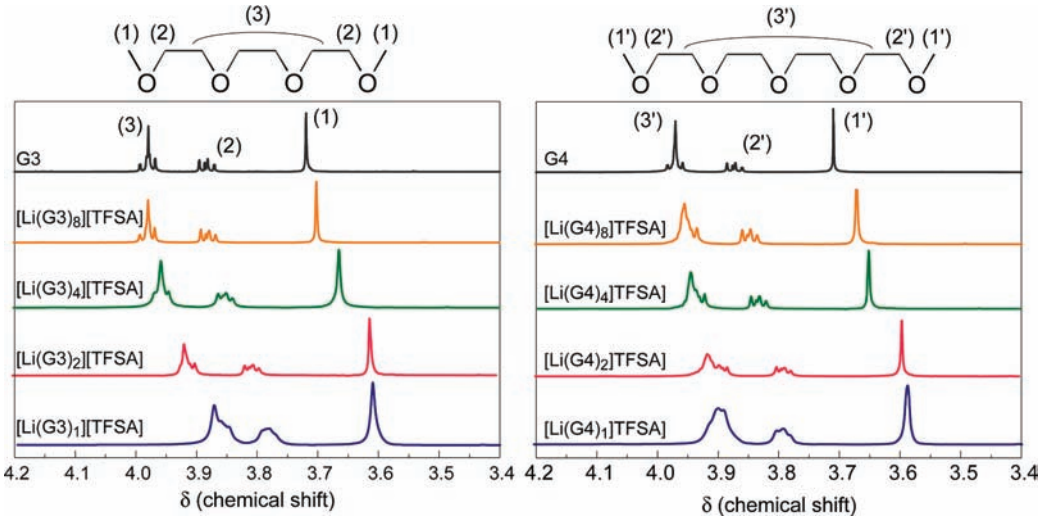

Figure 5. ^{1}H NMR spectra for pure glymes and [Li(glyme)$_x$][TFSA] (x = 1, 2, 4, and 8).

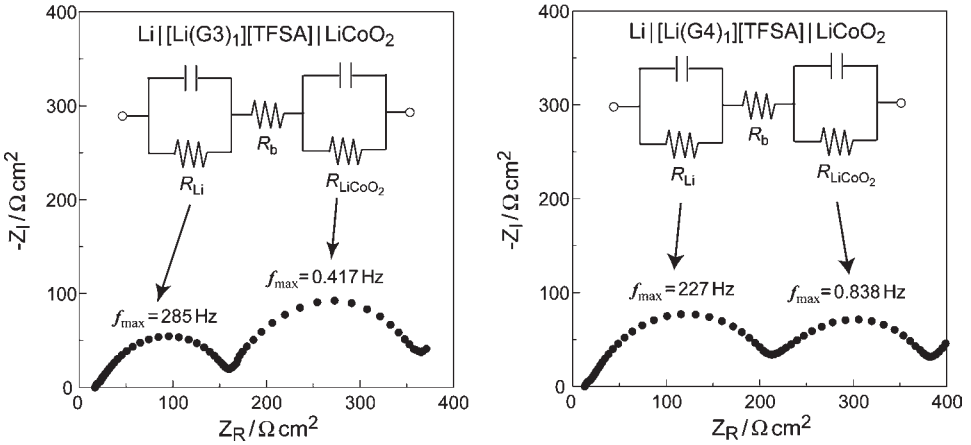

Figure 6. Nyquist plots for [Li metal anode|[Li(glyme)$_1$][TFSA]|LiCoO$_2$ cathode] cells measured at the cell voltage of 4 V at 30 °C.

interface can be estimated. The semicircle at the high-frequency range in Figure 6 is assigned to the charge-transfer process at the Li metal anode because the frequency range of the charge-transfer process observed for symmetric [Li|[Li(G3 or G4)$_1$]-[TFSA]|Li] coin-type cells (see Figure S2 in the Supporting Information) is similar to that of the high-frequency semicircle in Figure 6. The time constants for the charge-transfer process at the Li anode interface in [Li(G3)$_1$][TFSA] and [Li(G4)$_1$]-[TFSA] are 5.6 × 10^{-4} and 7.0 × 10^{-4} s, respectively. The semicircle at the low-frequency range in Figure 6 is assigned to the charge-transfer process at the LiCoO$_2$ cathode. The time constants for the LiCoO$_2$ cathode interface in [Li(G3)$_1$][TFSA] and [Li(G4)$_1$][TFSA] are 3.8 × 10^{-1} and 1.9 × 10^{-1} s, respectively. The rate-determining step of the charge-transfer process is considered to be the solvation/desolvation of the Li^+ cation at the interface.[65−67] Therefore, the time constant obtained from the electrochemical impedance can be regarded as the time scale of the formation and deformation of the complex cation [Li(glyme)$_1$]$^+$ at the interface in this study. The time constants for the Li anode are comparable to that of the lifetime in the [Li(glyme)$_2$][TFSA] solution. On the other hand, the time constants for LiCoO$_2$ cathode interfaces are in the range of 10^{-1} s and much larger than the lifetime of a free glyme in the bulk solution. Even in the [Li(glyme)$_2$][TFSA] solution containing much excess free glyme, the lifetime of the free glyme is in the range of 10^{-4} s. These results strongly support the hypothesis that the free-glyme molecule generated at the LiCoO$_2$ cathode interface receives immediately another Li^+ cation from the neighboring [Li(glyme)$_1$]$^+$ complex cation and forms again a complex before the oxidation process of free glyme occurs.

Combining the results of charge−discharge cycle tests, electrochemical impedance measurements for [Li anode|[Li(glyme)$_1$][TFSA]|LiCoO$_2$ cathode] cells, and ^{1}H NMR of the [Li(glyme)$_x$][TFSA] solution, it can be concluded that the Li^+ cation conduction by the ligand exchange mechanism, like the Grotthuss mechanism in acidic aqueous solutions, overlaps with the conventional migration mechanism of the [Li(glyme)$_1$]$^+$ cation in the equimolar [Li(glyme)$_1$][TFSA] complexes when the electrochemical reactions at the anode and cathode occur, and no free-glyme molecules exist within the cell during charge and discharge. This is probably true in the case of charge−discharge at a relatively low current density, that is, small perturbation from the equilibrium. Because the charge-transfer process at the interface can be accelerated by a large overpotential, the generation rate of free glymes may complete with the ligand exchange rate of [Li(glyme)$_1$]$^+$ as the discharge rate increases.

4. CONCLUSIONS

The electrochemical oxidation limit of the [Li(G3 or G4)$_x$][TFSA] solution shifted to a more positive electrode potential as the molar ratio of glyme x decreased. The equimolar complex [Li(glyme)$_1$][TFSA] was stable close to 5 V vs Li/Li$^+$, while the solutions containing excess glyme molecules ([Li(glyme)$_x$][TFSA], $x > 1$) were oxidized at around 4 V vs Li/Li$^+$. The oxidative stability of a glyme molecule was greatly enhanced by the formation of a complex cation [Li(glyme)$_1$]$^+$. This enhancement was due to the donation of lone pairs of ether oxygen atoms to the Li$^+$ cation, resulting in a lowering of the HOMO energy level of the glyme molecule, which was confirmed by ab initio molecular orbital calculations. The lifetime of a free glyme molecule in [Li(glyme)$_x$][TFSA] ($1 < x < 2$) is estimated to be in the order of 10^{-4} s. This lifetime is considerably shorter than the time constants for the interfacial charge-transfer process at the $LiCoO_2$ cathode in the [Li(glyme)$_1$][TFSA] equimolar complex. These results strongly suggested that Li$^+$ cation conduction in the [Li(glyme)$_1$][TFSA] equimolar complex occurs as a result of the ligand exchange in addition to the migration of a [Li(glyme)$_1$]$^+$ cation and a [TFSA]$^-$ anion. The ligand exchange conduction mode is induced by electrode reactions in a [Li anode | [Li(glyme)$_1$][TFSA] | $LiCoO_2$ cathode] cell. Because of the enhancement of the oxidative stability of glyme caused by the equimolar complexation with Li[TFSA], the battery could be operated for more than 200 charge−discharge cycles in the cell voltage range of 3.0−4.2 V regardless of the use of ether-based electrolytes.

■ ASSOCIATED CONTENT

Supporting Information. Figure S1 (HF/6-311G** level optimized geometry for the $[Li_2(G4)_2]^{2+}$ complex), Table S1 (Cartesian coordinates and calculated energy at the HF/6-311G** level), Table S2 (ionic conductivity of [Li(glyme)$_x$][TFSA] measured at 30 °C), Figure S2 (Nyquist plots for [Li|[Li(G3 or G4)$_1$][TFSA]|Li] cells), and complete ref 51. This material is available free of charge via the Internet at http://pubs.acs.org.

■ AUTHOR INFORMATION

Corresponding Author
mwatanab@ynu.ac.jp

■ ACKNOWLEDGMENT

This study was supported in part by a Technology Research Grant Program from the New Energy and Industrial Technology Development Organization (NEDO) of Japan, by a Grant-in-Aid for Scientific Research from the MEXT of Japan in the priority area "Science of Ionic Liquids" (#452/17073009), and by the ALCA program of Japan Science and Technology Agency (JST).

■ REFERENCES

(1) Armand, M. B.; Chabagno, J. M.; Duclot, M. J. *Fast Ion Transport in Solids*; Elsevier: New York, 1979; p 131.
(2) MacCallum, J. R., Vincent, C. A., Eds. *Polymer Electrolyte, Reviews − 1 and 2*; Elsevier Applied Science: London, 1987 and 1989.
(3) Nishimoto, A.; Agehara, K.; Furuya, N.; Watanabe, T.; Watanabe, M. *Macromolecules* **1999**, *32*, 1541.
(4) Nishimoto, A.; Watanabe, M.; Ikeda, Y.; Kojiya, S. *Electrochim. Acta* **1998**, *43*, 1177.
(5) Tobishima, S.; Morimoto, H.; Aoki, M.; Saito, Y.; Inose, T.; Fukumoto, T.; Kuryu, T. *Electrochim. Acta* **2004**, *49*, 979.
(6) Amine, K.; Wang, Q.; Vissers, D. R.; Zhang, Z.; Rossi, N. A. A.; West, R. *Electrochem. Commun.* **2006**, *8*, 429.
(7) Chen, Z.; Wang, H. H.; Vissers, D. R.; Zhang, L.; West, R.; Lyons, L. J.; Amine, K. *J. Phys. Chem. C* **2008**, *112*, 2210.
(8) Abraham, K. M.; Jiang, Z.; Carroll, B. *Chem. Mater.* **1997**, *9*, 1978.
(9) Tarascon, J.-M.; Armand, M. *Nature* **2001**, *414*, 359.
(10) Armand, M.; Tarascon, J.-M. *Nature* **2008**, *451*, 652.
(11) Goodenough, J. B.; Kim, Y. *Chem. Mater.* **2009**, *29*, 587.
(12) Seki, S.; Kobayashi, Y.; Miyashiro, H.; Yamanaka, A.; Mita, Y.; Iwahori, T. *J. Power Sources* **2005**, *146*, 741.
(13) Niitani, T.; Shimada, M.; Dokko, K.; Rho, Y.-H.; Kanamura, K. *Electrochem. Solid-State Lett.* **2005**, *8*, A385.
(14) Xu, K. *Chem. Rev.* **2004**, *104*, 4303.
(15) Sato, T.; Masuda, G.; Takagi, K. *Electrochim. Acta* **2004**, *49*, 3603.
(16) Ue, M.; Takeda, M.; Toriumi, A.; Kominato, A.; Hagiwara, R.; Ito, Y. *J. Electrochem. Soc.* **2003**, *150*, A499.
(17) Noda, A.; Susan, M. A. B. H.; Kubo, K.; Mitsushima, S.; Hayamizu, K.; Watanabe, M. *J. Phys. Chem. B* **2003**, *107*, 4024.
(18) Nakamoto, H.; Watanabe, M. *Chem. Commun.* **2007**, *24*, 2539.
(19) Lee, S.-Y.; Ogawa, A.; Kanno, M.; Nakamoto, H; Yasuda, T.; Watanabe, M. *J. Am. Chem. Soc.* **2010**, *132*, 9764.
(20) Kubo, W.; Kambe, S.; Nakade, S.; Kitamura, T.; Hanabusa, K.; Wada, Y.; Yanagida, S. *J. Phys. Chem. B* **2003**, *107*, 4374.
(21) Wang, P.; Zakeeruddin, S.; Moser, J.-E.; Grätzel, M. *J. Phys. Chem. B* **2003**, *107*, 13280.
(22) Kawano, R.; Watanabe, M. *Chem. Commun.* **2003**, *3*, 330.
(23) Garcia, B.; Lavallée, S.; Perron, G.; Michot, C.; Armand, M. *Electrochim. Acta* **2004**, *49*, 4583.
(24) Matsumoto, H.; Sakaebe, H.; Tatsumi, K. *J. Power Sources* **2005**, *146*, 45.
(25) Sakaebe, H.; Matsumoto, H.; Tatsumi, K. *J. Power Sources* **2005**, *146*, 693.
(26) Seki, S.; Kobayashi, Y.; Miyashiro, H.; Ohno, Y.; Mita, Y.; Usami, A.; Terada, N.; Watanabe, M. *Electrochem. Solid-State Lett.* **2005**, *8*, A577.
(27) Seki, S.; Kobayashi, Y.; Miyashiro, H.; Ohno, Y.; Usami, A.; Mita, Y.; Kihira, N.; Watanabe, M.; Terada, N. *J. Phys. Chem. B* **2006**, *110*, 10228.
(28) Seki, S.; Kobayashi, Y.; Miyashiro, H.; Ohno, Y.; Usami, A.; Mita, Y.; Watanabe, M.; Terada, N. *Chem. Commun.* **2006**, *5*, 544.
(29) Matsumoto, H.; Sakaebe, H.; Tatsumi, K.; Kikuta, M.; Ishiko, E.; Kono, M. *J. Power Sources* **2006**, *160*, 1308.
(30) Seki, S.; Ohno, Y.; Kobayashi, Y.; Miyashiro, H.; Usami, A.; Mita, Y.; Tokuda, H.; Watanabe, M.; Hayamizu, K.; Tsuzuki, S.; Hattori, M.; Terada, N. *J. Electrochem. Soc.* **2007**, *154*, A173.
(31) Fernicola, A.; Croce, F.; Scrosati, B.; Watanabe, T.; Ohno, H. *J. Power Sources* **2007**, *174*, 342.
(32) Seki, S.; Ohno, Y.; Miyashiro, H.; Kobayashi, Y.; Usami, A.; Mita, Y.; Terada, N.; Hayamizu, K.; Tsuzuki, S.; Watanabe, M. *J. Electrochem. Soc.* **2008**, *155*, A421.
(33) Seki, S.; Kobayashi, Y.; Miyashiro, H.; Ohno, Y.; Mita, Y.; Terada, N.; Charest, P.; Guerfi, A.; Zaghib, K. *J. Phys. Chem. C* **2008**, *112*, 16708.
(34) Borgei, V.; Markevich, E.; Aurbach, D.; Semrau, G.; Schmidt, M. *J. Power Sources* **2009**, *189*, 331.
(35) Tachikawa, N.; Park, J.-W.; Yoshida, K.; Tamura, T.; Dokko, K.; Watanabe, M. *Electrochemistry* **2010**, *5*, 349.
(36) Park, J.-W.; Yoshida, K.; Tachikawa, N.; Dokko, K.; Watanabe, M. *J. Power Sources* **2011**, *196*, 2264.
(37) Shobukawa, H.; Tokuda, H.; Tabata, S.; Watanabe, M. *Electrochim. Acta* **2004**, *50*, 304.
(38) Shobukawa, H.; Tokuda, H.; Susan, M. A. B. H.; Watanabe, M. *Electrochim. Acta* **2005**, *50*, 3872.
(39) Tamura, T.; Hachida, T.; Yoshida, K.; Tachikawa, N.; Dokko, K.; Watanabe, M. *J. Power Sources* **2010**, *195*, 6095.
(40) Henderson, W. A.; Brooks, N. R.; Brennessel, W. W.; Young, V. G., Jr. *Chem. Mater.* **2003**, *15*, 4679.

(41) Henderson, W. A.; Brooks, N. R.; Young, V. G., Jr. *Chem. Mater.* **2003**, *15*, 4685.
(42) Henderson, W. A.; Mckenna, F.; Kahn, M. A.; Brooks, N. R.; Young, V. G., Jr.; Frech, R. *Chem. Mater.* **2005**, *17*, 2284.
(43) Henderson, W. A. *J. Phys. Chem. B* **2006**, *110*, 13177.
(44) Gadjourova, Z.; Andreev, Y. G.; Tunstall, D. P.; Bruce, P. G. *Nature* **2001**, *412*, 520.
(45) Christie, A. M.; Lilley, S. J.; Staunton, E.; Andreev, Y. G.; Bruce, P. G. *Nature* **2005**, *433*, 50.
(46) Zhang, C.; Lilley, S. J.; Ainsworth, D.; Staunton, E.; Andreev, Y. G.; Slawin, A. M. Z.; Bruce, P. G. *Chem. Mater.* **2005**, *17*, 2284.
(47) Zhang, C.; Ainsworth, D.; Andreev, Y. G.; Bruce, P. G. *J. Am. Chem. Soc.* **2007**, *129*, 8700.
(48) Zhang, C.; Andreev, Y. G.; Bruce, P. G. *Angew. Chem., Int. Ed.* **2007**, *46*, 2848.
(49) Zhang, C.; Gamble, S.; Ainsworth, D.; Slawin, A. M. Z.; Andreev, Y. G.; Bruce, P. G. *Nat. Mater.* **2009**, *8*, 580.
(50) Tamura, T.; Yoshida, K.; Hachida, T.; Tsuchiya, M.; Nakamura, M.; Kazue, Y.; Tachikawa, N.; Dokko, K.; Watanabe, M. *Chem. Lett.* **2010**, *39*, 753.
(51) Frisch, M. J.; et al. *Gaussian 03*, revision D.01; Gaussian, Inc.: Wallingford, CT, 2004.
(52) Tokuda, H.; Hayamizu, K.; Ishii, K.; Susan, M. A. B. H.; Watanabe, M. *J. Phys. Chem. B* **2004**, *108*, 16593.
(53) Tokuda, H.; Hayamizu, K.; Ishii, K.; Susan, M. A. B. H.; Watanabe, M. *J. Phys. Chem. B* **2005**, *109*, 6103.
(54) Tokuda, H.; Ishii, K.; Susan, M. A. B. H.; Tsuzuki, S.; Watanabe, M. *J. Phys. Chem. B* **2006**, *110*, 2833.
(55) Tokuda, H.; Tsuzuki, S.; Susan, M. A. B. H.; Hayamizu, K.; Watanabe, M. *J. Phys. Chem. B* **2006**, *110*, 19593.
(56) Pedersen, C. J. *J. Am. Chem. Soc.* **1967**, *89*, 7017.
(57) Xia, Y.; Fujieda, T.; Tatsumi, K.; Prosini, P. P.; Sakai, T. *J. Power Sources* **2001**, *92*, 234.
(58) Krause, L. J.; Lamanna, W.; Summerfield, J.; Engle, M.; Korba, G.; Loch, R.; Atanasoski, R. *J. Power Sources* **1997**, *68*, 320.
(59) Kanamura, K. *J. Power Sources* **1999**, *81*−*82*, 123.
(60) Kanamura, K.; Umegaki, T.; Shiraishi, S.; Ohashi, M.; Takehara, Z. *J. Electrochem. Soc.* **2002**, *149*, A185.
(61) Peng, C.; Yang, L.; Zhang, Z.; Tachibana, K.; Yang, Y. *J. Power Sources* **2007**, *173*, 510.
(62) Kreuer, K. D.; Rabenau, A.; Wepperner, W. *Angew. Chem., Int. Ed. Engl.* **1982**, *21*, 208.
(63) Allerhand, A.; Gutowsky, H. S.; Jonas, J.; Meinzer, R. A. *J. Am. Chem. Soc.* **1966**, *88*, 3185.
(64) Orrell, K. G.; Šik, V.; Stephenson, D. *Prog. Nucl. Magn. Reson. Spectrosc.* **1990**, *22*, 141.
(65) Abe, T.; Fukuda, H.; Iriyama, Y.; Ogumi, Z. *J. Electrochem. Soc.* **2004**, *151*, A1120.
(66) Yamada, Y.; Iriyama, Y.; Abe, T.; Ogumi, Z. *Langmuir* **2009**, *25*, 12766.
(67) Yamada, Y.; Sagane, F.; Iriyama, Y.; Abe, T.; Ogumi, Z. *J. Phys. Chem. C* **2009**, *113*, 14528.